Machine Learned Coarse Grain Water Models for Evaporation Studies

Sumith Yesudasan,*,† Rodney D. Averett,‡ and Sibi Chacko¶

†*Department of Engineering Technology, Sam Houston State University, Huntsville, TX, USA*

‡*School of Chemical, Materials, and Biomedical Engineering, University of Georgia, Athens, GA, USA*

¶*School of Engineering and Physical Science, Heriot Watt University, Academic City, Dubai, UAE*

E-mail: sumith.yesudasan@shsu.edu

Abstract

Evaporation studies of water using classical molecular dynamics simulations are largely limited due to its high computational expense. We aim at addressing the computational issues by developing a coarse grain model for evaporation of water on solid surfaces by combining four water molecules into a single bead. Most commonly used mono atomic pair potentials like Lennard Jones, Morse, Mie and three body potential like Stillinger-Weber are optimized using a combination of Genetic algorithm and Nelder-Mead algorithm. Among them, Stillinger-Weber based model shows excellent agreement of density and Enthalpy of vaporization with experimental results for a wide range of temperatures. Further, the new water model is used to simulate contact angle of water and thin film evaporation from surfaces with different wettabilities.

Keywords: Coarse Grain Models; Water Models; Nanoscale Evaporation; Nano Channels; Molecular Dynamics

Preprints (www.preprints.org) | NOT PEER-REVIEWED | Posted: 7 July 2020 doi:10.20944/preprints202007.0126.v1

Introduction

With the advent of super computers and data center based cloud computing, the energy consumption of electronic sector has significantly increased over the past decade and the trend will continue. This demands compact designs with higher energy density and hence calls for highly efficient and faster cooling systems. The cooling system of a data center typically consumes around 40% of the energy input. This forecast to around $150 billion per year cost by the year 2030[1] and hence efficient cooling systems becomes a hot topic to research. Of many conventional cooling techniques, evaporative water cooling stands out as a best candidate due to its high specific heat capacity and high enthalpy of vaporization. Based on kinetic theory,[2] an evaporative heat flux of 20,000 W/cm^2 can be achieved using water at 1 atm. However, even with the recent developments in Nano-scale fabrication techniques the maximum heat flux is limited to 500 to 1000 W/cm^2.[3] This points out to our poor understanding of the nanoscale and microscale evaporation of water.

While experimental techniques pose challenges to validate and characterize the nanoscale phenomena, the computational tools like molecular dynamics can give promising results without the need for expensive machines and instrumentation. Studies show that thin film evaporation has high potential to remove heat compared to bulk region.[4,5] To study and extend these studies further, we need computational models with accurate representation of water and reproducibility of experimental results.

Studying water evaporation at nanoscale using experiments is a challenging attempt. Use of molecular dynamics can become helpful in this scenario,[6–8] however, to date, there is no single water model which can capture or simulate all of its properties.[9] Even the best performing and widely used models like SPCE[10] and TI3P[9] are unsuitable to study evaporation, due to the computational cost. This shifts our focus to computationally faster models called coarse grain molecular dynamics (CGMD) models.

In a typical CGMD model, one or more water molecules are combined into a bead or a super-molecule to represent the bulk properties of the system. Most of the existing CGMD

Preprints (www.preprints.org) | NOT PEER-REVIEWED | Posted: 7 July 2020 doi:10.20944/preprints202007.0126.v1

models are developed for bio-molecular studies[11–16] and is not tested for heat transfer. The existing CGMD models[13,17] mainly focus on the room temperature behavior of water or even sometimes the behavior below zero degree Celsius. While these models can capture freezing, ice formation and other properties of water,[18] their applicability to high temperature applications is limited or seldom. The field of coarse graining itself is a big research area and hence the readers are advised to refer consolidated reviews found elsewhere.[19–21] Among various types of CGMD models, mono bead models are appealing due to its very low computational power consumption.[11,22,23] Specifically the generalized Mie potential model[23] which maps one water molecule to a single bead can accurately represent density, surface tension and enthalpy of vaporization of water at a wide range of temperatures. Compared to this generalized Mie potential model, classical MARTINI model[11,22] combines 4 water molecules into one bead, which makes it computationally efficient.

In this work, we have utilized the combination of meta-heuristic[24] Genetic Algorithm (GA)[24] and Nelder-Mead (NM) method[25] for finding the optimum values of force field[26] parameters. The first step is GA in which the initial sample population is created randomly and optimization is performed by imitating natural selection, cross-over, mutation and reproduction.[27] The process is repeated until the best cost value reaches a threshold or upon reaching certain number of iterations. If the cost is not converged within the conditions set then the NM is initiated with an initial simplex.[25] The simplex is iteratively moved in the multi dimensions in direct search of the optimum parameters and terminates when the standard deviation of the simplex reaches a threshold or upon reaching certain number of iterations. The optimized force field parameters are then tested for reproducibility and its thermodynamic properties in the temperature range of $0°C$ to $170°C$. Our machine learning results show Stillinger-Weber (SW) potential simulates density and Enthalpy of vaporization and agrees with the experimental results accurately.

The machine learned Stillinger Weber (MLSW) model is used to study the contact angle of water droplet on the surface of a platinum plate. The interaction parameters between

Preprints (www.preprints.org) | NOT PEER-REVIEWED | Posted: 7 July 2020 doi:10.20944/preprints202007.0126.v1

the platinum and the MLSW beads are tuned to simulate hydrophobic and hydrophilic surfaces. Further, the thin film of water evaporation from the platinum surface is simulated and characterized for various wettability conditions.

Coarse Grain Models

The concept of coarse-grained (CG) modeling originates back from the 1970s.[28] Coarse-grained models assume various levels of reduced representation of the molecules, most of the time combining a bunch of atoms into a bead (as shown in Fig. 1) . These beads may be interconnected using bonds representing bio molecular chains or can be solo particles representing a fluid medium like water. The field of coarse grain molecular dynamics is broad and discussion of the methods is beyond the scope of this article. A few review papers discussing the recent innovations in the development of CG models, which broadly include structure-based, knowledge-based, and dynamics-based approaches can be found in the literature.[29,30]

The most widely used CG model is called MARTINI model,[11] which originally developed to simulate lipid molecules.[22] The MARTINI force field maps four heavy atoms to one CG interaction site and is parameterized to reproduce the thermodynamic properties. Simulating water heat transfer or evaporation using original MARTINI model as it is will produce incorrect results, but it is re-parameterized to the temperatures near 100 °C.[31]

A number of coarse grain models for water have emerged recently with the developments in the machine learning and artificial intelligence field.[18,32,33] Among them, we have selected the most widely used and classical potential models for mono atomic beads. They are (i) Morse,[34] (ii) Mie,[35] (iii) Lennard-Jones (LJ)[36] using pair interactions and (iv) Stillinger-Weber[37] based on three body interaction.

Preprints (www.preprints.org) | NOT PEER-REVIEWED | Posted: 7 July 2020 doi:10.20944/preprints202007.0126.v1

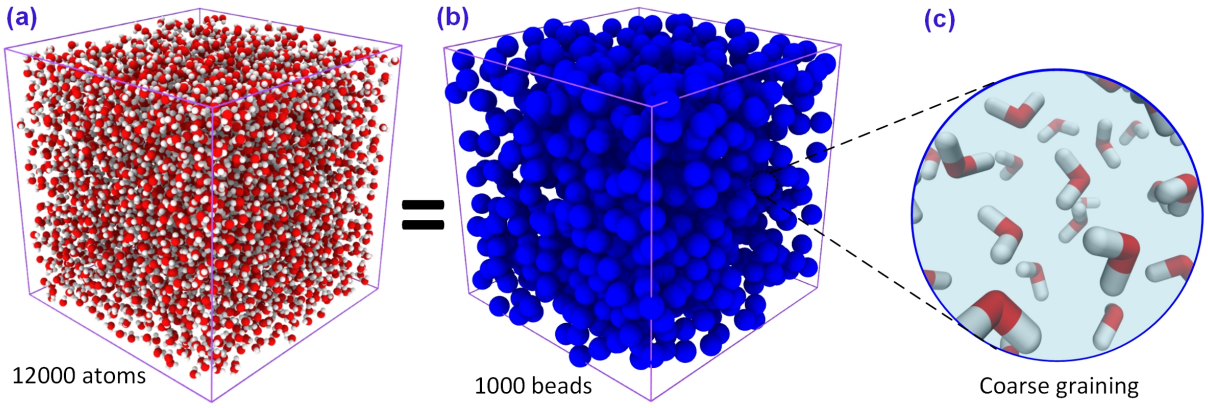

Figure 1: Coarse grain modeling of water. (a) water molecules in a 5 nm cubic box, (b) coarse grained water beads for the same cubic volume, (c) contents of one water bead (4 water molecules)

Morse Potential

The Morse potential, is a convenient inter atomic interaction model for a diatomic molecule. It is a better approximation for the vibrational structure of the molecule than the quantum harmonic oscillator[38] because it explicitly includes the effects of bond breaking, such as the existence of unbound states[34] . Though it was originally developed for diatomic molecules, the Morse potential can also be used to model other interactions such as the interaction between an atom and a surface.

$$U_{Morse}(r) = D_0 \left[e^{-2\alpha(r-r_0)} - 2e^{-\alpha(r-r_0)}\right] \tag{1}$$

The Morse potential energy function takes the form as shown in the Eqn. 1. Here r is the distance between the atoms, r_0 is the equilibrium distance, D_0 is the potential well depth, and α controls the spread of the potential function For numerical simulations, often a shift and a linear term is added to the potential so that both, potential energy and force, go to zero at the cut-off radius (Eqn. 2). Generally a cutoff radius is used to speed up the calculation using computer, so that atom pairs which distances are greater than the cutoff have an interaction energy of zero.

Preprints (www.preprints.org) | NOT PEER-REVIEWED | Posted: 7 July 2020 doi:10.20944/preprints202007.0126.v1

$$U_{Morseshift}(r) = U_{Morse}(r) - U_{Morse}(r_c) - (r - r_c)\frac{dU}{dr}\Big|_{r=r_c} \tag{2}$$

Mie Potential

Mie potential was proposed by Gustav Mie in 1903.[35] The functional form of Mie potential is given as in Eqn. 3. When $\gamma_R = 12$ and $\gamma_A = 6$ then Mie potential becomes a standard Lennard Jones potential. The Mie potential is investigated to represent CG model of water to match the vapor pressure and liquid-vapor co-existence.[23]

$$U_{Mie}(r) = C\epsilon\left[\left(\frac{\sigma}{r}\right)^{\gamma_R} - \left(\frac{\sigma}{r}\right)^{\gamma_A}\right] \tag{3}$$

Here, σ is the value of r at $U_{Mie}(r) = 0$, ϵ is the well depth (energy) and the constant C is given by the Eqn. 4. Also, γ_R and γ_A are the constants controlling the repulsive and attractive strength of the potential.

$$C = \left(\frac{\gamma_R}{\gamma_R - \gamma_A}\right)\left(\frac{\gamma_R}{\gamma_A}\right)^{\gamma_A/(\gamma_R - \gamma_A)} \tag{4}$$

Lennard Jones Potential

Lennard Jones (LJ) potential[36] developed by John Lennard-Jones in 1924, may be the most used inter atomic potential across all force fields in computational chemistry. The mathematical form of the potential is simple as given in the Eqn. 5 and has only two parameters to fit the thermodynamic properties of the fluid with experimental data.

$$U_{LJ126}(r) = 4\epsilon\left[\left(\frac{\sigma}{r}\right)^{12} - \left(\frac{\sigma}{r}\right)^{6}\right] \tag{5}$$

A variation of LJ potential for van der Waals interactions used in computer simulations of organic compounds, molecular liquids and divalent metal cations, is the COMPASS force field.[39] The potential takes the functional form as given in the Eqn. 6.

Preprints (www.preprints.org) | NOT PEER-REVIEWED | Posted: 7 July 2020 doi:10.20944/preprints202007.0126.v1

$$U_{LJ96}(r) = \epsilon \left[2 \left(\frac{\sigma}{r} \right)^9 - 3 \left(\frac{\sigma}{r} \right)^6 \right] \tag{6}$$

Here, in both cases, σ is the value of r at $U(r) = 0$, ϵ is the energy well depth.

Stillinger Weber Potential

The Stillinger-Weber (SW) potential[37] has a two-body and three-body terms of the standard form as shown in the Eqn. 7.

$$E = \sum_i \sum_{j>i} \phi_2(r_{ij}) \sum_i \sum_{j \neq i} \sum_{k>j} \phi_3(r_{ij}, r_{ik}, \theta_{ijk}) \tag{7}$$

The two body interaction term is ϕ_2 and is given in Eqn. 8.

$$\phi_2(r_{ij}) = A_{ij}\epsilon_{ij} \left[B_{ij} \left(\frac{\sigma_{ij}}{r_{ij}} \right)^{p_{ij}} - \left(\frac{\sigma_{ij}}{r_{ij}} \right)^{q_{ij}} \right] \exp \left(\frac{\sigma_{ij}}{r_{ij} - a_{ij}\sigma_{ij}} \right) \tag{8}$$

The three body interaction term is ϕ_3 and is given by Eqn. 9.

$$\phi_3(r_{ij}, r_{ik}, \theta_{ijk}) = \lambda_{ijk}\epsilon_{ijk} \left[\cos\theta_{ijk} - \cos\theta_{0ijk} \right]^2 \exp \left(\frac{\gamma_{ij}\sigma_{ij}}{r_{ij} - a_{ij}\sigma_{ij}} \right) \exp \left(\frac{\gamma_{ik}\sigma_{ik}}{r_{ik} - a_{ik}\sigma_{ik}} \right) \tag{9}$$

The SW potential is originally created for simulating Silicon metal interaction, however later has been extended to simulate other elements and also water.[18,40] The readers are advised to refer the original Stillinger Weber research paper[37] for the nomenclature and details of the parameters shown in Eqns 7, 8, 9.

Genetic Algorithm

The potential models described in the previous sections are used to map four water molecules into a CG bead, just like the standard MARTINI model.[11] This means, a CG bead represents 12 atoms which can significantly reduce the computational cost. To have a consistent

Preprints (www.preprints.org) | NOT PEER-REVIEWED | Posted: 7 July 2020 doi:10.20944/preprints202007.0126.v1

comparison among different potentials, 4 water molecules are mapped to a bead for Mie, Morse, LJ 12-6, LJ 9-6 and SW potential models. For every model, the initial population (parameters) are created based on the original atomic or CG versions with a 10% spread using a uniformly distributed random noise using MATLAB.[41] This random population is used to search for an optimized parameter set using Genetic Algorithm.

Genetic algorithm (GA) is a meta-heuristic inspired by the process of natural selection that belongs to the larger class of evolutionary algorithms (EA). Genetic algorithm is commonly used to optimization and search problems by relying on biologically inspired operators such as mutation, crossover and selection. For our work, the selection, pairing, mating and mutations are performed based on the textbook by Haupt and Ellen.[42] The selection rate is 50% and mutation rate is 20%. The mating step follows the BLX-α method.[43] The population size is selected as 50, and maximum number of generations is set as 200. To save the computational effort, the iterative process is stopped when $cost_{GA}$ value falls below 5% or the standard deviation of 10 consecutive cost values falls less than 1%. The steps involved in the parameter search using GA is shown in the Fig. 2a.

All Coarse Grain Molecular Dynamics (CGMD) simulations are performed using LAMMPS software.[44] The temperature and pressure is controlled using a Nose-Hoover thermostat and barostat[45–47] with a chain length of four. The simulations start with an energy minimization for 1000 steps, followed by equilibration runs of 50,000 steps and production runs of 50,000 steps. The time step of integration is chosen as $5fs$ which is relatively low compared to a standard CGMD simulation. Number of steps for equilibration and production are selected based on the time required for the equilibration of energy, temperature and pressure and the standard deviations of energy and temperature is within 1%. The cut off radius for all the simulations are taken as 12Å, same as the original MARTINI model.

The density is estimated using a liquid cubic system of 1000 beads using NPT ensemble, which is pre-equilibrated for a density of $1000kg/m^3$. The Enthalpy of vaporization is estimated based on both liquid cubic system of 1000 beads (density of $1000kg/m^3$) and vapor

Preprints (www.preprints.org) | NOT PEER-REVIEWED | Posted: 7 July 2020 doi:10.20944/preprints202007.0126.v1

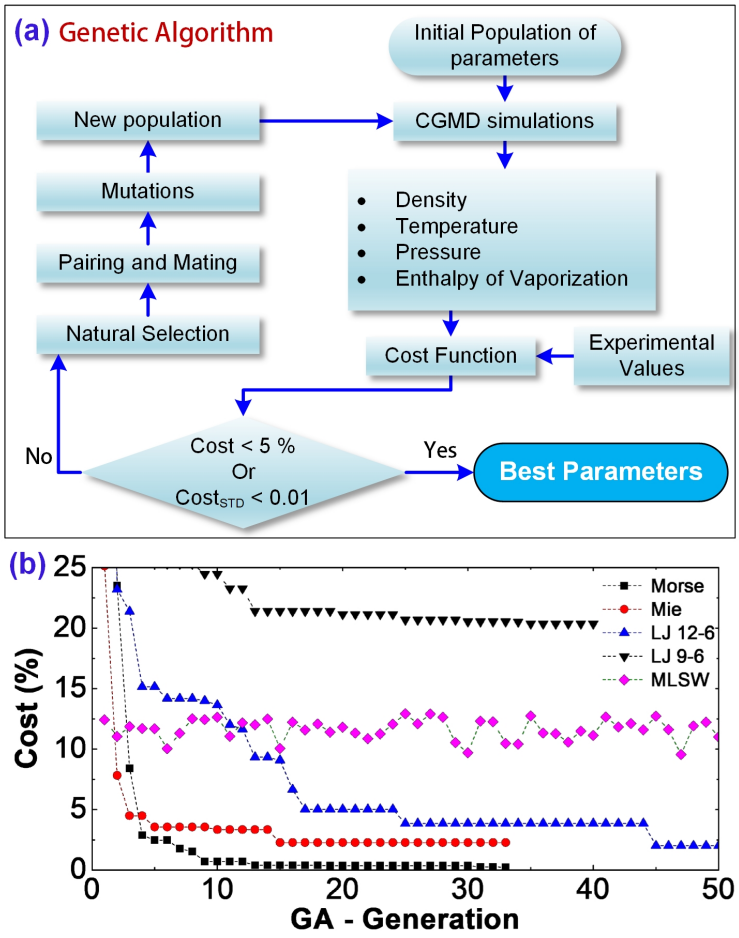

Figure 2: (a) Steps involved in implementing Genetic Algorithm for CG model parameter search. (b) Nelder-Mead Optimization process for the CG model parameter search.

Preprints (www.preprints.org) | NOT PEER-REVIEWED | Posted: 7 July 2020 doi:10.20944/preprints202007.0126.v1

cubic system of 200 beads at a density of $2kg/m^3$.

From the simulations, density and Enthalpy of vaporization of the systems are estimated at 100 °C and compared to the experimental values from the NIST standard web book.[48] This comparison is made using a percentage error based cost function as described in the Eqn. 10. Initially, surface tension values of water was also included in the optimization loop. However, since it lead to a never converging scenario, we excluded the surface tension from the list.

$$cost_{GA} = \frac{100}{D} \sum_{i}^{D} \frac{|\psi^i_{EXP} - \psi^i_{CGMD}|}{\psi^i_{EXP}} \tag{10}$$

Here, ψ represents the quantities (density and enthalpy) to compare with experimental results, subscripts EXP and $CGMD$ means the values from experiments and simulations respectively. The summation runs from i to D, which represents the number of quantities used to compare (2 in our case). Thus obtained cost values for each CG water models are shown in Fig. 2b. The legends represents the corresponding CG water models with MLSW being Machine Learned Stillinger-Weber model.

Table 1: Optimized parameters of various potential models using genetic algorithm

	ϵ or D_0	σ or r_0	γ_R	γ_A	α	$cost_{GA}$ (%)
Mie	1.354595	4.707993	6.297204	8.326509	-	2.26
Morse A	1.692254	5.8106	-	-	0.625373	0.24
LJ 12-6	1.482684	4.737085	-	-	-	2.02
LJ 9-6	1.198251	4.729665	-	-	-	**20.36**

The MLSW potential parameters corresponding to the final $cost_{GA}$ value of **17.36%** is $\epsilon = 8.412576\,(kcal/mol)$, $\sigma = 2.743976\,(\text{Å})$, $a = 2.442725$, $\lambda = 10.653902$, $\gamma = 1.225309$, $cos\theta_0 = -0.240518$, $A = 4.334005$, $B = 2.986314$, $p = 5.006381$, $q = 0.192317$, $tol = 0.207676$. Here, tol is a LAMMPS specific term to improvise the speed of execution, using a virtual cutoff distance in constructing atom neighbor lists. The rest of the terms are same as given in the Eqns. 7, 8, 9.

Preprints (www.preprints.org) | NOT PEER-REVIEWED | Posted: 7 July 2020 doi:10.20944/preprints202007.0126.v1

The trend shows poor convergence for the LJ 9-6 and MLSW model with a best $cost_{GA}$ of 20.36% and 17.36% respectively. For all the models, its cost values corresponding to the generations is plotted in the Fig. 2b. The best cost values (final generation) of these models and the final parameters are listed out in Table 1. Note that at this stage the parameters are optimized based on the values corresponding to 100 °C. For a broader temperature range, only Morse and MLSW are promising ones (reason will be discussed in the results section) and the rest (LJ 12-6, LJ 9-6 and Mie) will be unsuitable.

Even though Genetic algorithm is an efficient technique, like in many problems, GA have a tendency to converge towards local optima or even arbitrary points rather than the global optimum of the problem. In such occassions, local optimization algorithms like Nelder-Mead[25] or Levenberg-Marquardt algorithm.[49] The SW models are proven to accommodate a broader temperature range[18] and hence we will further parameterize SW and Morse potential based CG models using NM algorithm as described in the next section.

Nelder-Mead Multi-Temperature Optimization

The Nelder–Mead (NM) method is a commonly applied numerical method[25,50] to find the minimum or maximum of an objective (cost) function in a multidimensional space. It is a direct search method and is often applied to nonlinear optimization problems for which derivatives may not be known. The method uses the concept of a simplex, which is a special polytope of $n + 1$ vertices in n dimensions. The major steps of this algorithm are sorting the simplex based on the objective function values, reflection, expansion, contraction and shrinking.

There exists many variations for the numerical implementation of NM method, of which we used the original method[25] to further optimize the parameters of Morse and MLSW potential based CG water models. The algorithm of NM implementation in our CG strategy is shown in Fig. 3. The final parameter set obtained from the GA optimization is used as the initial simplex for the iterative NM method.

Preprints (www.preprints.org) | NOT PEER-REVIEWED | Posted: 7 July 2020 doi:10.20944/preprints202007.0126.v1

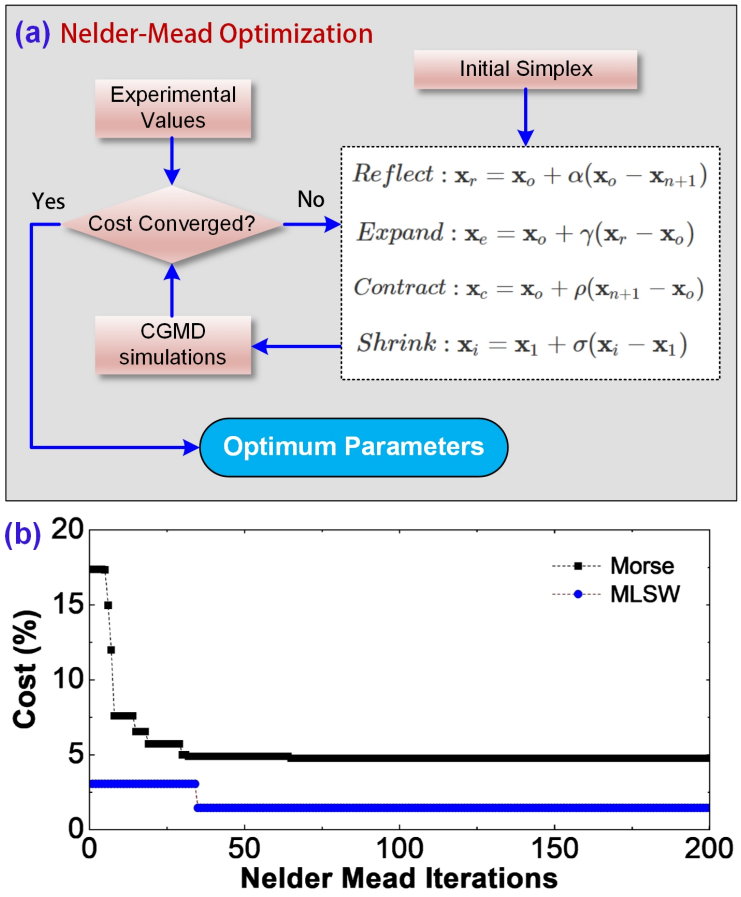

Figure 3: Results of GA and NM optimization of water models. (a) Cost function values of various potential functions versus GA population generations. (b) Best cost function values of MLSW and Morse potentials vs. optimization iterations.

Preprints (www.preprints.org) | NOT PEER-REVIEWED | Posted: 7 July 2020 doi:10.20944/preprints202007.0126.v1

The integration of NM method with the Coarse graining procedure is shown as in Fig. 3a. Based on the parameters (simplex) selected, the cost function is estimated using the Eqn. 11. This time, instead of comparing and optimizing the results for a single temperature, thermodynamic properties corresponding to four different temperatures are considered. This multi point (Temperatures of 0°C, 50°C, 100°C, 150°C) optimization will allow a better agreement of the CG model with the experimental results.

$$cost_{NM} = 100 \left[s_1 \sum_{i=1}^{4} \frac{|\rho_{exp,T_i} - \rho_{cgmd,T_i}|}{\rho_{exp,T_i}} + s_2 \sum_{i=1}^{4} \frac{|\Delta H_{exp,T_i} - \Delta H_{cgmd,T_i}|}{|\Delta H_{exp,T_i}|} \right] \tag{11}$$

Here, $cost_{NM}$ is the cost function value associated with the NM method, s_1 and s_2 are scales, ρ is density and ΔH is the enthalpy of vaporization corresponding to the temperature T. The subscript i runs from 1 to 4, representing $T_1 = 0°C$ to $T_4 = 150°C$. The scales (for our case, $s_1 = 0.25$ and $s_2 = 0.75$) are used for controlling the convergence between two quantities whose percentage error makes big difference in absolute error.

The cost function value associated with the NM optimization is shown in the Fig. 3b. Both CG models Morse and MLSW didn't show any further convergence after 50 iterations. The cost value at the 200^{th} iteration is 5.46% and 1.44% for Morse and MLSW respectively. The corresponding parameters of the Morse CG force field (Eqn. 2) and MLSW CG force field is shown in Table 2 and Table 3 respectively.

Table 2: Optimized parameters of Morse CG model

D_0 $(kcal/mol)$	α $(1/Å)$	r_0 (Å)
1.721406	1.051702	5.463566

Table 3: Optimized parameters of MLSW CG model

ϵ $(kcal/mol)$	σ (Å)	a	λ	γ	$\cos(\theta_0)$
7.379305	2.676254	2.416000	11.480988	1.209011	-0.269785
A	B	p	q	tol	
4.337364	2.278919	4.701969	0.231351	0.224757	

Preprints (www.preprints.org) | NOT PEER-REVIEWED | Posted: 7 July 2020 doi:10.20944/preprints202007.0126.v1

These are the final optimized parameters of the CG water models Morse and MLSW. In the next section, further validation of these models and sensitivity testings will be explained.

Machine Learned Models and Sensitivity Studies

The water CG models based on Mie, Lennard Jones, Morse and MLSW will be used to estimate the density, enthalpy of vaporization, and surface tension. These properties are estimated for the temperature range of $0^{\circ}C$ to $150^{\circ}C$ with an interval of $10^{\circ}C$. For every temperature, time step of integration is chosen as $5\,fs$, equilibrated for $50,000$ steps followed by $50,000$ steps of production runs. For getting a reliable data, 20 simulations are performed for every temperature points, each time with a different velocity distribution. The results from these simulations are shown in the Fig. 4.

Figure 4a shows the density variation of various CG models with respect to temperature. The bold line shows the experimental value obtained from NIST database.[48] The values corresponding to the CG models are plotted using a marker shown in the legend. The error bars of the data are not shown due to negligible variation and hence the average values are plotted. The results show a very good agreement of the MLSW model with the experimental density at all temperature ranges. The second best model is Morse.

The results from the CGMD simulations for the Enthalpy of vaporization is shown in the Fig. 4b and the results for the surface tension is shown in Fig. 4c. Though none of the models predict surface tension accurately with experimental results, MLSW and Morse based CG models show better performance than the rest. In fact, the main objective of our studies is to simulate heat transfer and phase change in nano channels. For such studies, the primary importance is to agree with properties like density and Enthalpy of vaporization, rather than surface tension. Especially, near the temperature of $100^{\circ}C$, the MLSW model and Morse model perform well for both density and ΔH, which makes them a good candidate for studying thin film heat transfer and evaporation.

Preprints (www.preprints.org) | NOT PEER-REVIEWED | Posted: 7 July 2020 doi:10.20944/preprints202007.0126.v1

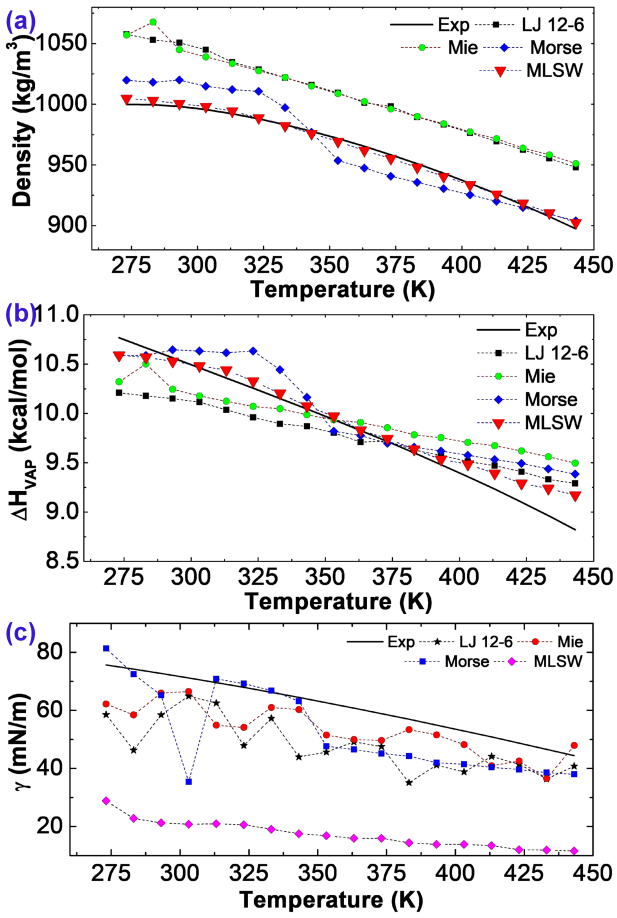

Figure 4: Results of various CGMD models with temperature. (a) Density variation of the LJ 12-6 (square), Mie (circle), Morse (diamond), MLSW (inverted triangle) compared with experimental results (solid line). (b) Enthalpy of vaporization variation of LJ 12-6 (square), Mie (circle), Morse (diamond), MLSW (inverted triangle) compared with experimental results (solid line) and (c) Surface tension variation of the LJ 12-6 (star), Mie (circle), Morse A (triangle), Morse (square), MLSW (diamond) compared with experimental results (solid line).

Preprints (www.preprints.org) | NOT PEER-REVIEWED | Posted: 7 July 2020 doi:10.20944/preprints202007.0126.v1

Sensitivity studies

The initial optimization of the parameters are based on the cutoff radius 1.2 nm, number of water molecules mapped into a bead as 4, and a time step of integration of 5 fs. Additional studies are performed to check how these simulation parameters affect the force field's ability to reproduce thermodynamic properties like density and Enthalpy. For MLSW, the cutoff radius is part of the potential function and is optimized as the part of the CG algorithm. For Morse, the cutoff radius sensitivity is tested by changing it to 1.2 nm , 1.8 nm and 2.2 nm. The resulting effect in the density and the Enthalpy is shown in the Fig. 5a and 5b respectively. The density and ΔH is very sensitive to the cutoff radius. Both quantities increase with increasing cutoff radius and hence won't be able to predict the correct thermodynamic properties.

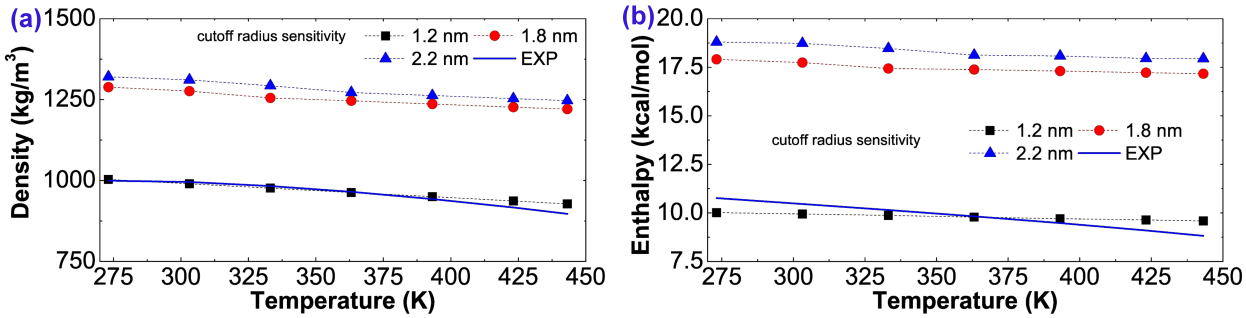

Figure 5: (a) Sensitivity of density with cutoff radius of Morse-A potential. (b) Sensitivity of Enthalpy of vaporization with cutoff radius of Morse-A potential.

To study the computational speed of various CG models, we varied the system size with 100 beads (12 nm^3) to 20,000 beads (1800 nm^3) at 400 K for 5,000 steps. The simulations are performed using LAMMPS[44] and the time consumed in seconds using a single processor is shown in Fig. 6a. The results show LJ 12-6 potential is fastest among the three. Despite of being a 3-body potential, MLSW is 7 to 22 % faster than the Morse depending on the system size.

The time step of integration is chosen in a way that it will have minimum impact in the total energy fluctuation. It was varied from $1fs$ to $100fs$. A temperature of $500K$ is

Preprints (www.preprints.org) | NOT PEER-REVIEWED | Posted: 7 July 2020 doi:10.20944/preprints202007.0126.v1

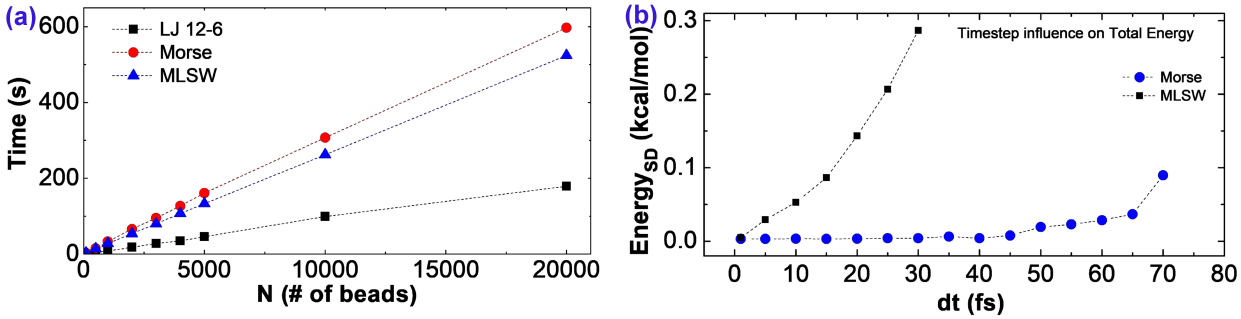

Figure 6: (a) Time consumption of different water CGMD models in a single processor vs. number of beads in the system. (b) Standard deviation of the total energy of the system with 1000 beads vs. time step of integration.

used for testing the sensitivity for higher temperatures, with a system size of 1000 beads, equilibrated for 50000 steps using NVT ensemble and production runs of 50000 using NVE ensemble. The standard deviations of total energy for Morse and MLSW cases are shown in the Fig. 6b. The system became unstable for Morse potential after $70fs$ and for MLSW after $40fs$. The ideal choice of time step for Morse potential can be somewhere between $30fs$ to $40fs$. On the other hand, the time step is sensitive with MLSW potential. Since our validation and optimization studies are performed at $5fs$, we will be using $5fs$ as the time step for the future studies using MLSW potential.

Based on our studies and analysis so far, MLSW predicts density and ΔH better than Morse potential. One might often be interested in simulating water using Morse potential due its simplicity in implementing. Hence, we used GA algorithm again to search for the optimum parameters with different cutoff radii, number of water molecules per bead, time step of integration etc. The maximum number of generations are set as 100, and the cases shown in the Table 4 is optimized for the temperature $100°C$ using GA. The corresponding results of different Morse models (A, B, C, D) are shown in Table 4, with the optimized cost in the last column.

Preprints (www.preprints.org) | NOT PEER-REVIEWED | Posted: 7 July 2020 doi:10.20944/preprints202007.0126.v1

Table 4: Morse potential parameters for different cutoff radii, coarse grain level and time steps

	D_0	r_0	r_{cut} (nm)	N_{wat}	α	dt (fs)	Cost (%)
Morse A	1.692254	5.8106	1.2	4	0.625373	1	0.23
Morse B	1.572749	5.431679	1.8	4	0.992873	1	1.42
Morse C	1.743659	6.893268	1.8	8	0.865287	1	1.34
Morse D	1.686345	5.8106	1.2	4	0.625349	30	**0.13**

Results and Discussion

In comparison with other machine learned coarse grained models, MLSW was able to reproduce the density, enthalpy of vaporization and surface tension better. Hence we chose MLSW model for studying the contact angle and thin film evaporation properties of water at various types of surfaces.

Contace angle of water droplet

A small water droplet of 5 nm^3 volume is placed on top of a platinum plate and equilibrated as shown in the Fig. 7a. This droplet represents 1000 MLSW beads, equivalent to 4000 water molecules on top of a FCC 100 platinum monolayer sheet. The molecular system have a dimension of $15nm \times 15nm \times 15nm$. The horizontal boundaries are periodic and vertical boundaries are reflective on top and fixed on bottom. The water beads and platinum sheet beads interact with a standard 12-6 Lennard-Jones potential (Eqn. 10). The droplet is equilibrated using LAMMPS software[44] for 500,000 steps with a time step of integration of 5 fs. The center of mass of the momentum is nullified throughout the simulation to avoid any drifting of the droplet from the center.

The equilibrated droplet is then used to simulate the contact angle of the water. The sigma (σ_{LJ}) parameter of the water-wall interaction is kept the same as that of a standard MARTINI model (0.47 nm) and the epsilon (ϵ_{LJ}) is varied from 0 $kcal/mol$ to 1 $kcal/mol$ at a 0.04 $kcal/mol$ increment. For all the studies, epsilon is kept at 0 for 50,000 steps, followed

Preprints (www.preprints.org) | NOT PEER-REVIEWED | Posted: 7 July 2020 doi:10.20944/preprints202007.0126.v1

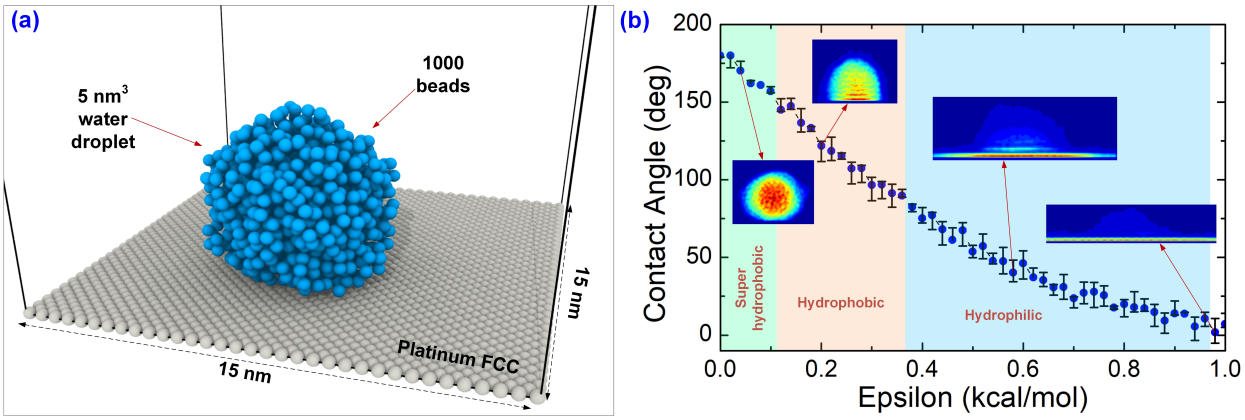

Figure 7: Contact angle studies of water droplet. (a) An equilibrated 5 nm^3 water droplet on the surface of a platinum FCC 100 monolayer sheet. (b) Influence of surface interaction parameter, epsilon (ϵ_{LJ}) and surface behavior. Simulation of super-hydrophobic, hydrophobic and hydrophilic surfaces based on varying epsilon.

by 500,000 steps of equilibration at appropriate epsilon and finally production run of 500,000 steps at 5 fs time step. The resulting trajectories are further analyzed using the contact angle estimation algorithm[51–53] to estimate the contact angle for various epsilons. For every epsilon 10 different initial velocity distributions are considered to account the statistical variation.

The contact angle values corresponding to the water-wall interaction parameter epsilon is shown in the Fig. 7b. The inset pictures show the snapshot of the droplets while using our contact angle algorithm. The results show a quadratic variation of the average contact angle values with epsilon parameter. The error bar indicates the maximum and minimum values due to the initial conditions. Based on the wettability[54] properties of a surface, it can be classified into super-hydrophobic (contact angle $> 150°$), hydrophobic (contact angle $> 90°$) and hydrophilic (contact angle $< 90°$). These three characteristics are able to reproduce for the water droplet through our simulations using MLSW water model and shown in the Fig. 7b.

Evaporation of thin water film

Using the contact angle study, we could identify the wall-water interaction parameters for creating super-hydrophobic, hydrophobic and hydrophilic surfaces. We extend this system

Preprints (www.preprints.org) | NOT PEER-REVIEWED | Posted: 7 July 2020 doi:10.20944/preprints202007.0126.v1

to further study evaporation of a thin water film and its effect on surface wettability[54] characteristics. Two parallel platinum (FCC 100) plates at 15 nm apart are taken with an MLSW water film of 6 nm thickness is equlibrated next to the lower plate as shown in the Fig. 8 a, b. The dimensions of the system are shown in the Fig. 8 b, and Fig. 8 a represents multiple periodic images to visualize the system. A width of 3.6 nm (3 times cutoff radius) is chosen to avoid any self-interaction of beads across periodic boundaries. The interaction of MLSW beads with each other is using MLSW potential (Table 3), and with the platinum wall is using LJ 12-6 potential. A time step of 5 fs is used for the studies with an equilibration of films for 300,000 steps (1.5 ns) at 300 K followed by a 300,000 steps (1.5 ns) of production runs at 400 K.

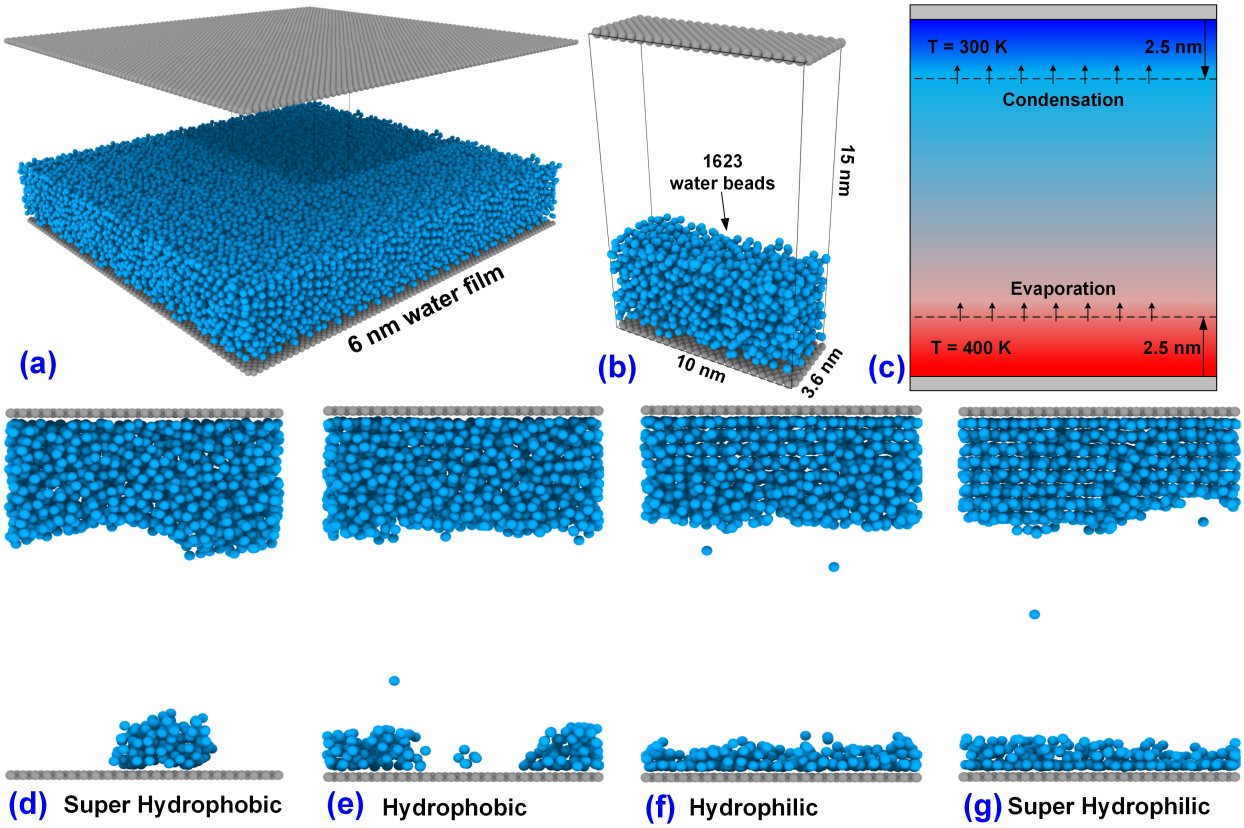

Figure 8: Evaporation of a thin film of water. (a) A 6 nm thick MLSW water film is equilibrated and placed in between platinum plates. (b) The system is 10 nm × 3.6 nm × 15 nm, with 1623 MLSW beads (6 nm thick). (c) Hot and cold regions of the system for evaporation and condensation is shown. Final evaporated thin film for (d) super-hydrophobic, (e) hydrophobic, (f) hydrophilic and (g) super-hydrophilic surfaces are shown.

Preprints (www.preprints.org) | NOT PEER-REVIEWED | Posted: 7 July 2020 doi:10.20944/preprints202007.0126.v1

To simulate the evaporation and condensation of the thin films, the aforementioned system is defined with heating and cooling regions as shown in the Fig. 8 c. The temperature of lower region is kept at 400 K and that of the upper region is maintained at 300 K using a simple velocity re-scaling algorithm. This temperature gradient led to a sudden jumping of half of the film from the lower region to upper plate. Eventually the remaining liquid film is evaporated and deposited on the top surface as shown in the Fig. 8 d-g, for various types of surface characteristics. Here, the super-hydrophobic case corresponds to an epsilon value of 0.04 kcal/mol, hydrophobic corresponds to 0.2 kcal/mol, hydrophilic corresponds to 0.6 kcal/mol and super-hydrophilic corresponds to 0.92 kcal/mol. The results show a layer like formation at higher epsilon values which as expected for nanoscale thin films,[55] due to strong wall-water interactions. The results show that hydrophobic surfaces are more favorable towards evaporation than the hydrophilic ones.

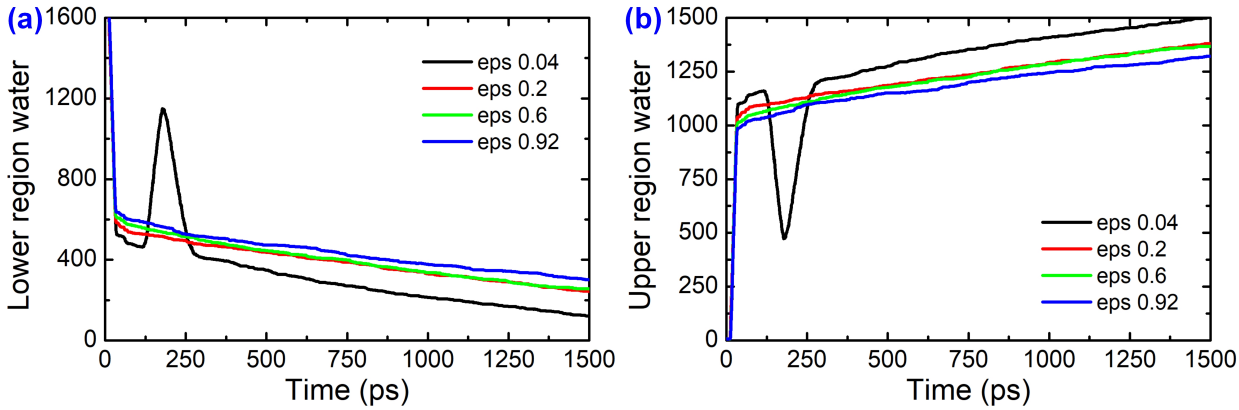

Figure 9: Time evolution of the MLSW beads during the evaporation and condensation of the thin film. (a) The evaporation of MLSW beads over time from the lower surface. (b) The condensation of the MLSW beads over time to the upper surface.

The quantification of the evaporation data using the trajectory evolution is done using a self written Python computer code and shown in Fig. 9. The Fig. 8 a shows the evaporation of the water from the lower region and 8 b shows the condensation of the film on the upper region. The figure shows the number of MLSW beads in the lower and upper regions by using a partition at 7.5 nm in the midsection of the system. The data shows increasing evaporation and condensation rates for increasing hydrophobicity of the surface. A sharp

 doi:10.20944/preprints202007.0126.v1

jump in the graphs around 200 ps is due to the bounce back of the film from the upper surface and then continued evaporation.

Conclusion

In this work we used the most commonly used molecular force fields to develop the best coarse grain model to perform evaporation studies of water at nano to micro scale. We combined 4 water molecules into a coarse grained bead and using machine learning algorithms we examined Lennard-Jones potential, Morse potential, Mie potential and Stillinger-Weber (SW) potential and their suitability to reproduce the experimental properties of water. We found that Morse and SW potentials performs better than the rest with SW potential performing well across a wide range of temperatures. Using the Machine Learned Stillinger Weber (MLSW) water model, we performed the contact angle and thin film evaporation studies at surfaces with different wettabilities. The contact angle studies were used to determine the wall-water interaction parameters to simulate hydrophobic and hydrophilic surfaces. The evaporation study simulated the thin film of water evaporating from a surface and condensing to another platinum surface. The surface wettability characteristics of this platinum surface was tuned and evaporation was performed at hydrophobic and hydrophilic surfaces. The results show a favorable evaporating condition with the hydrophobic surfaces. We believe this study will serve as the first coarse grain water evaporation study and in the future multiscale and mesoscale studies of water at complex geometries can be performed with minimal computational expenditure.

References

(1) Andrae, A. S.; Edler, T. On global electricity usage of communication technology: trends to 2030. *Challenges* **2015**, *6*, 117–157.

(2) Gambill, W.; Lienhard, J. An upper bound for the critical boiling heat flux. *ASME J. Heat Transfer* **1989**, *111*, 815–818.

(3) Jaikumar, A.; Rishi, A.; Gupta, A.; Kandlikar, S. G. Microscale morphology effects of copper–graphene oxide coatings on pool boiling characteristics. *Journal of Heat Transfer* **2017**, *139*, 111509.

(4) Bigham, S.; Fazeli, A.; Moghaddam, S. Physics of microstructures enhancement of thin film evaporation heat transfer in microchannels flow boiling. *Scientific reports* **2017**, *7*, 44745.

(5) Wang, Q.; Chen, R. Ultrahigh flux thin film boiling heat transfer through nanoporous membranes. *Nano letters* **2018**, *18*, 3096–3103.

(6) Akkus, Y.; Beskok, A. Molecular diffusion replaces capillary pumping in phase-change-driven nanopumps. *Microfluidics and Nanofluidics* **2019**, *23*, 14.

(7) Akkus, Y.; Koklu, A.; Beskok, A. Atomic Scale Interfacial Transport at an Extended Evaporating Meniscus. *Langmuir* **2019**, *35*, 4491–4497.

(8) YD, S.; Maroo, S. C. Surface-Heating Algorithm for Water at Nanoscale. *The Journal of Physical Chemistry Letters* **2015**, *6*, 3765–3769.

(9) Jorgensen, W. L.; Chandrasekhar, J.; Madura, J. D.; Impey, R. W.; Klein, M. L. Comparison of simple potential functions for simulating liquid water. *The Journal of chemical physics* **1983**, *79*, 926–935.

(10) Berendsen, H.; Grigera, J.; Straatsma, T. The missing term in effective pair potentials. *Journal of Physical Chemistry* **1987**, *91*, 6269–6271.

(11) Marrink, S. J.; Risselada, H. J.; Yefimov, S.; Tieleman, D. P.; De Vries, A. H. The MARTINI force field: coarse grained model for biomolecular simulations. *The journal of physical chemistry B* **2007**, *111*, 7812–7824.

(12) Murtola, T.; Falck, E.; Patra, M.; Karttunen, M.; Vattulainen, I. Coarse-grained model for phospholipid/cholesterol bilayer. *The Journal of chemical physics* **2004**, *121*, 9156–9165.

(13) Vishnyakov, A.; Mao, R.; Lee, M.-T.; Neimark, A. V. Coarse-grained model of nanoscale segregation, water diffusion, and proton transport in Nafion membranes. *The Journal of chemical physics* **2018**, *148*, 024108.

(14) Yesudasan, S.; Wang, X.; Averett, R. D. Molecular dynamics simulations indicate that deoxyhemoglobin, oxyhemoglobin, carboxyhemoglobin, and glycated hemoglobin under compression and shear exhibit an anisotropic mechanical behavior. *Journal of Biomolecular Structure and Dynamics* **2018**, *36*, 1417–1429.

(15) Yesudasan, S.; Wang, X.; Averett, R. D. Coarse-grained molecular dynamics simulations of fibrin polymerization: effects of thrombin concentration on fibrin clot structure. *Journal of molecular modeling* **2018**, *24*, 109.

(16) Yesudasan, S.; Wang, X.; Averett, R. D. Fibrin polymerization simulation using a reactive dissipative particle dynamics method. *Biomechanics and modeling in mechanobiology* **2018**, *17*, 1389–1403.

(17) Raubenolt, B.; Gyawali, G.; Tang, W.; Wong, K.; Rick, S. Coarse-grained simulations of aqueous thermoresponsive polyethers. *Polymers* **2018**, *10*, 475.

(18) Chan, H.; Cherukara, M. J.; Narayanan, B.; Loeffler, T. D.; Benmore, C.; Gray, S. K.; Sankaranarayanan, S. K. Machine learning coarse grained models for water. *Nature communications* **2019**, *10*, 379.

(19) Hadley, K. R.; McCabe, C. Coarse-grained molecular models of water: a review. *Molecular simulation* **2012**, *38*, 671–681.

(20) Riniker, S.; Allison, J. R.; van Gunsteren, W. F. On developing coarse-grained models for biomolecular simulation: a review. *Physical Chemistry Chemical Physics* **2012**, *14*, 12423–12430.

(21) Brini, E.; Algaer, E. A.; Ganguly, P.; Li, C.; Rodríguez-Ropero, F.; van der Vegt, N. F. Systematic coarse-graining methods for soft matter simulations–a review. *Soft Matter* **2013**, *9*, 2108–2119.

(22) Marrink, S. J.; De Vries, A. H.; Mark, A. E. Coarse grained model for semiquantitative lipid simulations. *The Journal of Physical Chemistry B* **2004**, *108*, 750–760.

(23) Lobanova, O.; Avendaño, C.; Lafitte, T.; Müller, E. A.; Jackson, G. SAFT-γ force field for the simulation of molecular fluids: 4. A single-site coarse-grained model of water applicable over a wide temperature range. *Molecular Physics* **2015**, *113*, 1228–1249.

(24) Goldberg, D. Genetic algorithms in search, optimization, and machine learning, addison-wesley, reading, ma, 1989. *NN Schraudolph and J* **1989**, *3*.

(25) Nelder, J. A.; Mead, R. A simplex method for function minimization. *The computer journal* **1965**, *7*, 308–313.

(26) Leach, A. R.; Leach, A. R. *Molecular modelling: principles and applications*; Pearson education, 2001.

(27) Mitchell, M. *An introduction to genetic algorithms*; MIT press, 1998.

(28) Levitt, M.; Warshel, A. Computer simulation of protein folding. *Nature* **1975**, *253*, 694–698.

(29) Pak, A. J.; Voth, G. A. Advances in coarse-grained modeling of macromolecular complexes. *Current opinion in structural biology* **2018**, *52*, 119–126.

(30) Singh, N.; Li, W. Recent Advances in Coarse-Grained Models for Biomolecules and Their Applications. *International journal of molecular sciences* **2019**, *20*, 3774.

(31) Yesudasan, S. Extended MARTINI water model for heat transfer studies. *Molecular Physics* **2019**, 1–9.

(32) Wang, J.; Olsson, S.; Wehmeyer, C.; Pérez, A.; Charron, N. E.; De Fabritiis, G.; Noé, F.; Clementi, C. Machine learning of coarse-grained molecular dynamics force fields. *ACS central science* **2019**, *5*, 755–767.

(33) Bejagam, K. K.; Singh, S.; An, Y.; Deshmukh, S. A. Machine-learned coarse-grained models. *The journal of physical chemistry letters* **2018**, *9*, 4667–4672.

(34) Morse, P. M. Diatomic molecules according to the wave mechanics. II. Vibrational levels. *Physical Review* **1929**, *34*, 57.

(35) Mie, G. Zur kinetischen Theorie der einatomigen Körper. *Annalen der Physik* **1903**, *316*, 657–697.

(36) Jones, J. E. On the determination of molecular fields.—II. From the equation of state of a gas. *Proceedings of the Royal Society of London. Series A, Containing Papers of a Mathematical and Physical Character* **1924**, *106*, 463–477.

(37) Stillinger, F. H.; Weber, T. A. Computer simulation of local order in condensed phases of silicon. *Physical review B* **1985**, *31*, 5262.

(38) Griffiths, D. J.; Schroeter, D. F. *Introduction to quantum mechanics*; Cambridge University Press, 2018.

(39) Sun, H. COMPASS: an ab initio force-field optimized for condensed-phase applications overview with details on alkane and benzene compounds. *The Journal of Physical Chemistry B* **1998**, *102*, 7338–7364.

(40) Molinero, V.; Moore, E. B. Water modeled as an intermediate element between carbon and silicon. *The Journal of Physical Chemistry B* **2008**, *113*, 4008–4016.

(41) MATLAB, *version 7.10.0 (R2010a)*; The MathWorks Inc.: Natick, Massachusetts, 2010.

(42) Haupt, R. L.; Ellen Haupt, S. Practical genetic algorithms. **2004**,

(43) Eshelman, L. J.; Schaffer, J. D. *Foundations of genetic algorithms*; Elsevier, 1993; Vol. 2; pp 187–202.

(44) Plimpton, S. *Fast parallel algorithms for short-range molecular dynamics*; 1993.

(45) Martyna, G. J.; Tuckerman, M. E.; Tobias, D. J.; Klein, M. L. Explicit reversible integrators for extended systems dynamics. *Molecular Physics* **1996**, *87*, 1117–1157.

(46) Martyna, G. J.; Tobias, D. J.; Klein, M. L. Constant pressure molecular dynamics algorithms. *The Journal of chemical physics* **1994**, *101*, 4177–4189.

(47) Shinoda, W.; Shiga, M.; Mikami, M. Rapid estimation of elastic constants by molecular dynamics simulation under constant stress. *Physical Review B* **2004**, *69*, 134103.

(48) Lemmon, E.; Huber, M.; McLinden, M. NIST Standard Reference Database 23: Reference Fluid Thermodynamic and Transport Properties-REFPROP, Version 9.1, Standard Reference Data Program. *National Institute of Standards and Technology: Gaithersburg, MD* **2013**,

(49) Levenberg, K. A method for the solution of certain non-linear problems in least squares. *Quarterly of applied mathematics* **1944**, *2*, 164–168.

(50) Lagarias, J. C.; Reeds, J. A.; Wright, M. H.; Wright, P. E. Convergence properties of the Nelder–Mead simplex method in low dimensions. *SIAM Journal on optimization* **1998**, *9*, 112–147.

(51) Yd, S.; Maroo, S. C. A New Algorithm for Contact Angle Estimation in Molecular Dynamics Simulations. 2015.

 doi:10.20944/preprints202007.0126.v1

(52) Daisy, S. Y.; Maroo, S. C. A robust algorithm for contact angle and interface detection of water and argon droplets. *Heat Transfer Engineering* **2017**, *38*, 1343–1353.

(53) Daisy, S. Y. An efficient algorithm for contact angle estimation in molecular dynamics simulations. *International Journal of Engineering* **2015**, *9*, 1–8.

(54) Shafrin, E. G.; Zisman, W. A. Constitutive relations in the wetting of low energy surfaces and the theory of the retraction method of preparing monolayers1. *The Journal of Physical Chemistry* **1960**, *64*, 519–524.

(55) Yesudasan Daisy, S. Molecular dynamics study of solid-liquid heat transfer and passive liquid flow. **2016**,

Preprints (www.preprints.org) | NOT PEER-REVIEWED | Posted: 7 July 2020 doi:10.20944/preprints202007.0126.v1

Graphical TOC Entry